Gas-Phase Conformation-Specific Photofragmentation of Proline-Containing Peptide Ions

Tae-Young Kim,* Stephen J. Valentine, David E. Clemmer, and James P. Reilly

Department of Chemistry, Indiana University, Bloomington, Indiana, USA

Singly-protonated proline-containing peptides with N-terminal arginine are photodissociated with vacuum ultraviolet (VUV) light in an ESI linear ion trap/orthogonal-TOF (LIT/o-TOF). When proline is the n^{th} residue from the N-terminus, unusual $b_n + 2$ and $a_n + 2$ ions are observed. Their formation is explained by homolytic cleavage of the $C_\alpha - C$ bond in conjunction with a rearrangement of electrons and an amide hydrogen. The latter is facilitated by a proline-stabilized gas-phase peptide conformation. (J Am Soc Mass Spectrom 2010, 21, 1455–1465) © 2010 American Society for Mass Spectrometry

Structural analysis of peptides and proteins in the gas phase provides insight into their intrinsic intramolecular interactions. Comparison of structural differences between the gas and solution phase should be helpful to understand the effects of solvents [1, 2]. The invention of matrix-assisted laser desorption/ionization (MALDI) [3] and electrospray ionization (ESI) [4] has greatly facilitated the application of mass spectrometry (MS) to investigations of gas-phase biomolecular structure. Hydrogen/deuterium (H/D) exchange in the gas phase has been employed to examine conformers of cytochrome *c* ions having different charge states [5–8] and the stability of noncovalent complexes of small biomolecules [9, 10]. Ion mobility experiments have provided size information on solvent-free biomolecular structures under different conditions by measuring their collision cross sections [11, 12]. Various mass spectrometric ion activation techniques have also been employed to probe conformations of peptides or proteins in the gas-phase. Electron capture dissociation (ECD) combined with thermal activation has revealed conformational changes involved in folding and unfolding processes of protein ions in the gas-phase [13, 14]. Information about gas-phase salt bridges between acidic and basic residues has been derived from the type and abundance of product ions generated by low-energy collision-induced dissociation (CID) [15, 16], surface-induced dissociation (SID) [17], blackbody infrared radiative dissociation (BIRD) [18], and photodissociation [19].

Proline has a significant effect on tertiary peptide or protein structure [20–22] and peptide fragmentation in tandem MS [23–25] because of its unique ring structure. The *cis* and *trans* forms of proline in the gas phase have been resolved by ion mobility spectrometry (IMS) [26]. It is well-known that peptide ions have a propensity to cleave N-terminal to proline [27–30]. Wysocki and coworkers have studied this with a database of low-energy CID tandem mass spectra of doubly-charged peptides [31]. They have found that the residue (Xxx) adjacent to proline affects the extent of fragmentation at the Xxx-Pro bond. Particularly enhanced Xxx-Pro bond cleavage when Xxx is Val, Ile, and Leu was ascribed to the steric hindrance of their bulky side chains, since it causes proline to take a 'reactive' *trans* form that leads to product ions. However, they did not elucidate the 'reactive' conformation of proline or the mechanism of fragmentation. Herein, we present vacuum ultraviolet (VUV) photodissociation tandem mass spectra of proline-containing peptide ions generated by ESI that contain some unusual product ions. Formation of these abnormal product ions can be understood by considering the effect that proline has on the gas-phase conformation of peptides. The capabilities of VUV photodissociation and IMS for studying the gas-phase structures of proline are also demonstrated with two prototypical proline-containing peptides (RVV**P**V and RLL**P**L).

Experimental

Materials

Angiotensin II and α-cyano-4-hydroxycinnamic acid (CHCA) were purchased from Sigma (St. Louis, MO, USA). Peptides RLEQFG, RSAASLNS, and RDL**P**FF**P**V**P**ID were obtained from Sigma-Genosys (Woodlands, TX, USA) and

Address reprint requests to Professor J. P. Reilly, Department of Chemistry, Indiana University, 800 E. Kirkwood Ave., Bloomington, Indiana, USA. E-mail: reilly@indiana.edu

* Current address: Division of Chemistry and Chemical Engineering, California Institute of Technology, Pasadena, California 91125, USA.

1044-0305/10/$32.00
doi:10.1016/j.jasms.2010.04.007

Published online April 18, 2010
Received February 24, 2010
Revised April 7, 2010
Accepted April 13, 2010

RVV**P**V and RLL**P**L were synthesized in-house on Wang resin using standard *N*-9-fluorenylmethyloxycarbonly (Fmoc) chemistry. Acetonitrile (ACN) and trifluoroacetic acid (TFA) were obtained from EMD Chemicals (Gibbstown, NJ, USA).

Photodissociation MS

Tandem mass spectrometry of ESI-generated ions was carried out in a hybrid mass spectrometer that connected a Thermo Scientific (San Jose, CA, USA) LTQ ion trap with a nano-ESI source orthogonally to a homemade reflectron time-of-flight (TOF) mass analyzer using an ion guide consisting of an rf-only octopole and a DC quadrupole. Five to 10 μmol peptide solutions with 1% acetic acid in methanol were infused into the ion trap at a flow rate of 200 nL/min. Photodissociation experiments are performed either inside the ion trap or in the TOF source since an F_2 laser (EX100HF-60, GAM Laser, Orlando, FL, USA) was aligned coaxially with the ion trap and through the TOF source. For photodissociation in the TOF source, singly-charged precursor ions were isolated inside the trap with a bandwidth of 0.7 Da. Ions were axially extracted to the TOF source by a pullout pulse. There they were coaxially irradiated by 157 nm laser light before orthogonal extraction into the TOF analyzer. A single 10 ns unfocused F_2 laser pulse with 2 mJ of energy and a 5 mm $\times$ 10 mm of cross section was used for photodissociation. Spectra with and without sample injection were separately recorded to subtract the photoionization contribution. Spectra were recorded with a 5 μs time delay between photoexcitation and orthogonal extraction in the TOF source. For photodissociation inside the ion trap, the laser light was introduced at the beginning of the activation step with normalized collision energy set to 0% and activation q of 0.1. CID experiments were performed with 35% normalized collision energy and an activation q of 0.25 without introduction of the laser light. Detailed descriptions of photodissociation in the ion trap [32] and TOF source [33] can be found elsewhere.

Photodissociation of MALDI-generated ions was performed in an Applied Biosystems (Foster City, CA, USA) 4700 Proteomics Analyzer modified for photodissociation with an F_2 laser (Lambda Physik, Göttingen, Germany). Detailed information about the instrument has been presented elsewhere [34]. MALDI samples were prepared by mixing the peptide solution with matrix solution (10g/L CHCA in 1:1 (vol/vol) water/ACN solution with 0.1% TFA) in 1:9 (vol/vol) ratio, then 0.5 μL of analyte/matrix solution was deposited on each MALDI spot.

IMS MS

Solutions of the peptides RVV**P**V and RLL**P**L were electrosprayed into the IMS-MS instrument. Estimated peptide ion concentrations were 100 μM. Briefly, ions from the ESI source are trapped in an electrodynamic ion funnel as described previously [35]. Periodically (31.1 ms), ions are extracted into a drift tube (1.83 m long) containing ~2.9 torr of He buffer gas. The drift field is maintained at ~10 V/cm during the mobility measurements. Mobility-dispersed ions exiting the drift tube are focused into an orthogonally-extracted TOF source for mass analysis. Measured drift times are used to determine collision cross sections for all dataset features.

Mobility selection of peptide ions and ion activation are achieved as described previously [36]. Briefly, a voltage pulse (50 μs wide) is applied to an ion gating region in the middle of the drift tube. This pulse is delayed by a determined amount of time from the initial drift pulse and allows transmission of ions of selected mobilities; all others are neutralized on the gate grid. Ion activation of selected ions is achieved by applying a high field to a short (~3 mm) region immediately after the selection gate.

Molecular Dynamics Simulations

To aid interpretation of the IMS distributions for $[RVV\mathbf{P}V + H]^+$ and $[RLL\mathbf{P}L + H]^+$, molecular dynamics simulations have been performed using the InsightII software suite (Accelrys Inc., San Diego, CA, USA). The simulations have focused on the types of gas-phase conformations formed from *cis*- and *trans*-configurations of the proline residue. Two simulated annealing/dynamics cycles have been employed for each stereoisomer configuration leading to a total of eight analyses. The extensible systematic force field (ESFF) has been employed in all simulations and a dielectric of 1.0 has been used.

Each cycle simulates peptide ion configurations over a period of 9 ns. Briefly, a linear peptide ion is heated from 298 to 500 K over 5 ps (step 1). Dynamics are performed at 500 K for 50 ps (step 2). Next, the ion is cooled to 298 K over 5 ps (step 3), and subsequently dynamics are performed for 30 ps at 298 K (step 4). Time increments of 0.2 and 1 fs are used in the dynamics calculations for steps 1 through 3, and 4, respectively. The peptide ion structure is then energy-minimized and stored and the heating process is started again. This is repeated 100 times to generate an ensemble of structures. Collision cross sections are calculated for the trial structures using the Mobcal program that has been described previously [37, 38]. To ensure adequate sampling, a second round of annealing is employed using low-energy, matching (collision cross section) precursor structures from the first analysis. The second cycle uses gentler heating conditions (400 K). A torsion angle restraint is used to prevent conversion of the *cis*- to the *trans*-configuration of the proline residue.

Results and Discussion

Unusual b + 2 and a + 2 Ions Associated with Proline

Photodissociation of singly-protonated peptides with N-terminal arginine by VUV light in a MALDI tandem

TOF instrument yields high-energy *a*- and *d*-type ions [39]. These results led us to propose that 157 nm light induces homolytic radical cleavage between the α- and carbonyl-carbons that generates $a + 1$ radical ions [40]. Subsequent loss of a hydrogen atom ($H\cdot$) at the β-carbon or the amide backbone nitrogen generates *a*-type ions [41]. Tandem mass spectra of typical peptides RLEQFG and RSAASLNS obtained by 157 nm photodissociation in the TOF source of a linear ion trap/orthogonal-TOF (LIT/o-TOF) mass spectrometer with an ESI source are displayed in Figure 1a and b, respectively. As in previous MALDI tandem TOF mass spectra, the main products are *a*- and *d*-type ions. Some *b*- and *c*-type ions are also observed with relatively low intensities. Interestingly, $a + 1$ radical ions are more intense than the adjacent *a*-type ions for high *m/z* product ions ($a_4 + 1$ and $a_5 + 1$ in Figure 1a, and $a_5 + 1$, $a_6 + 1$, and $a_7 + 1$ in Figure 1b). Although $a + 1$

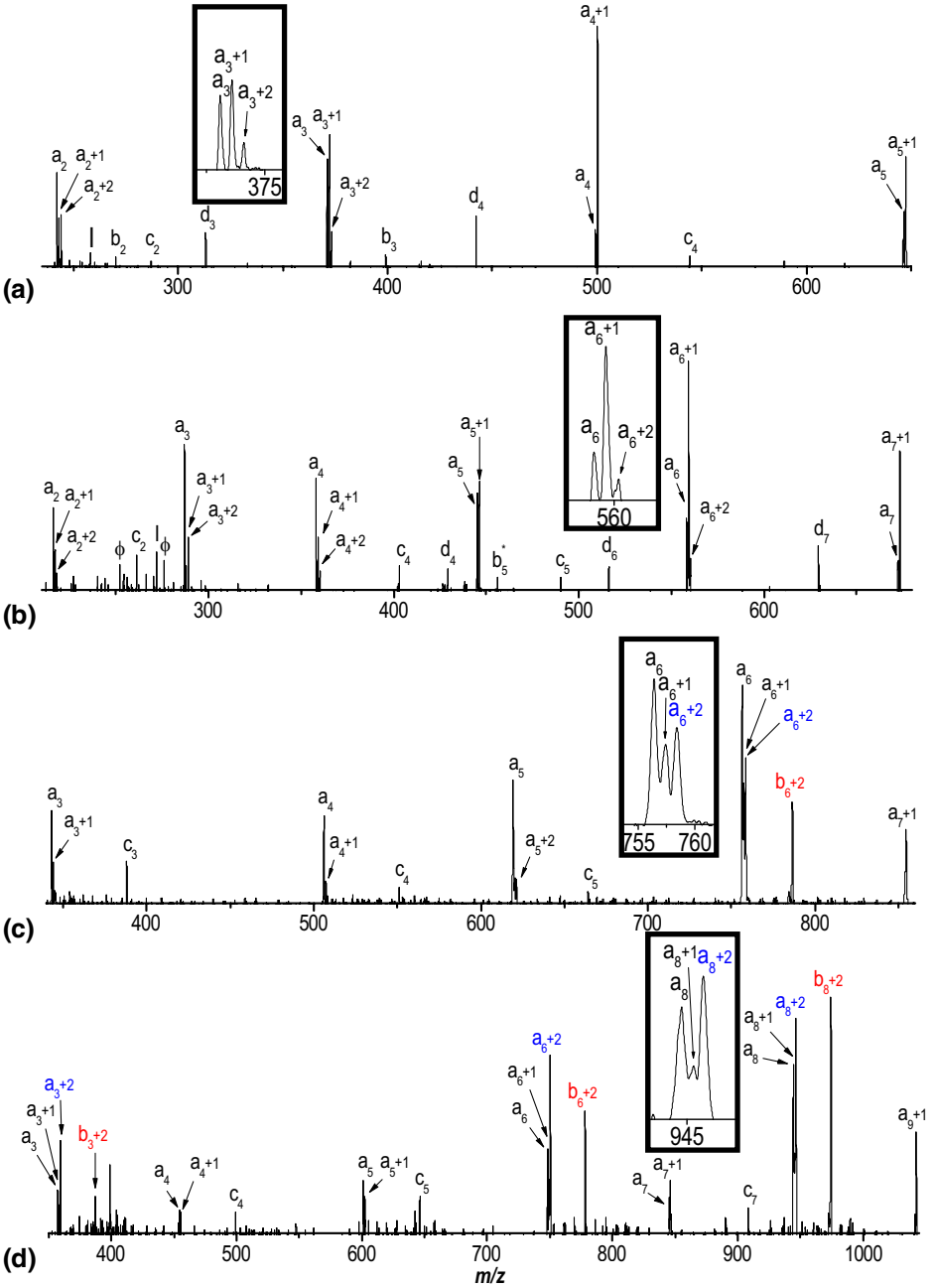

Figure 1. Tandem mass spectra recorded by 157 nm photodissociation of singly-protonated (**a**) RLEQFG, (**b**) RSAASLNS, (**c**) DRVYIH**P**F (angiotensin II), and (**d**) RDL**P**FF**P**V**P**ID in LIT/o-TOF mass spectrometer with a time delay of 5 μs between laser irradiation and ion extraction in the TOF source. The insets represent the peak intensity distributions of a, $a + 1$, and $a + 2$ ions typical for non-proline- and proline-associated *a*-type ions. Internal fragments, photoions, and loss of NH_3 are indicated by I, Φ, and *, respectively.

radical ions were also detected in the MALDI tandem TOF mass spectra, they were less intense than their *a*-ion counterparts. Presumably, radical ions have a better chance to survive when precursor ions have lower internal energies. Considering that $a + 1$ ions are the primary products from 157 nm photodissociation of N-terminal charge-containing peptides and *a* ions are formed by the loss of H ·, the formation of $a + 2$ ions by the H · capture or rearrangement is not expected. In ECD experiments, this type of unit mass increase for odd-electron $z \cdot$ ions was observed for peptide ions in a low charge state [42]. Likewise, $a + 2$ product ions can be produced by VUV photodissociation of N-terminal arginine-containing peptides (e.g., $a_2 + 2$ and $a_3 + 2$ in Figure 1a, and $a_2 + 2$, $a_3 + 2$, $a_4 + 2$, and $a_6 + 2$ in Figure 1b), but their peak intensities are generally low. However, in the photodissociation mass spectra of N-terminal arginine-containing peptides having proline residues in their sequences, $a + 2$ ions terminated by a residue N-terminal to proline can be abnormally intense. Data for peptides DRVYIH**P**F and RDL**P**FF**P**V**P**ID are presented in Figure 1c and d. Peak $a_6 + 2$ in Figure 1c and peaks $a_3 + 2$, $a_6 + 2$ and $a_8 + 2$ in Figure 1d are all very large. Even more remarkably, they are accompanied by corresponding $b + 2$ ions ($b_6 + 2$ in Figure 1c, and $b_3 + 2$, $b_6 + 2$, and $b_8 + 2$ in Figure 1d). We are not aware of any previous reports of $b + 2$ ions in tandem mass spectra.

Factors Affecting Formation of Abnormal b + 2 *and* a + 2 *Ions*

To investigate the origin of these ions, peptide DRVYIH**P**F was also collisionally dissociated and photodissociated inside the LIT. As shown in Figure 2a, neither $a_6 + 2$ nor $b_6 + 2$ ions are produced by CID. However both appear in the photodissociation MS^2 spectrum of Figure 2b. This illustrates that $b_6 + 2$ ions are uniquely formed by the photodissociation process. The difference between the two photodissociation tandem mass spectra (Figure 1c and

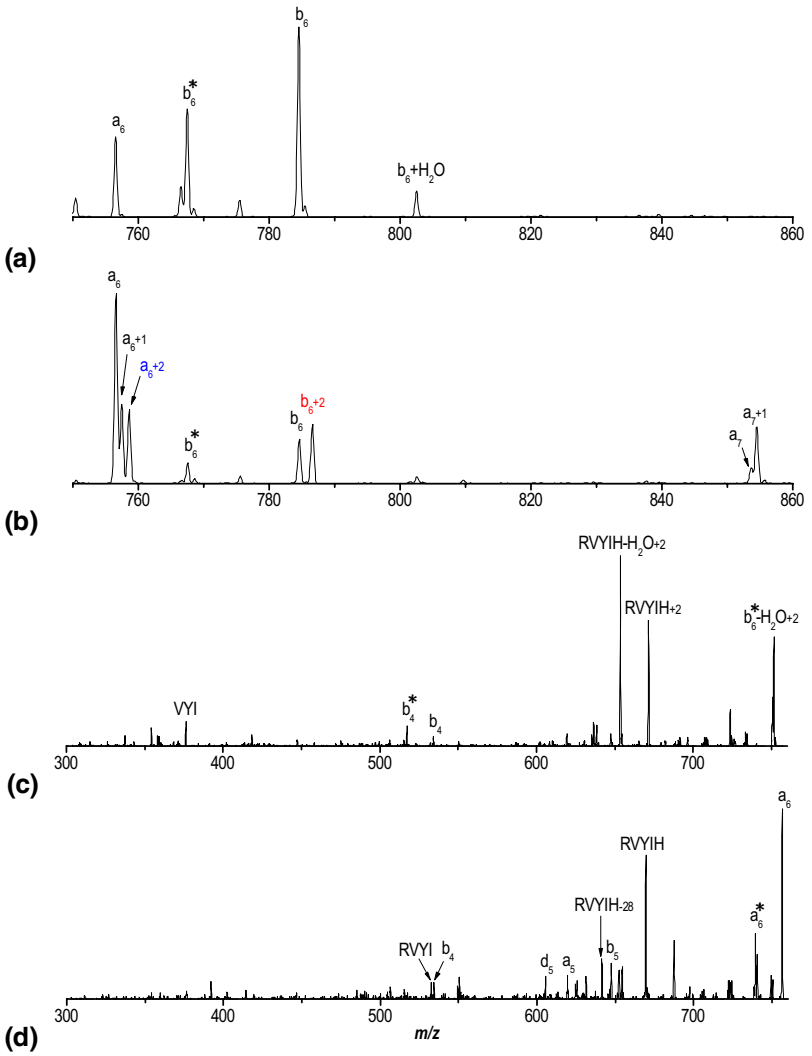

Figure 2. Expanded MS^2 mass spectra of DRVYIH**P**F (angiotensin II) around 800 *m/z* obtained by (**a**) CID and (**b**) 157 nm photodissociation in the ion trap of LIT/o-TOF mass spectrometer. CID MS^3 mass spectra of (**c**) $b_6 + 2$ and (**d**) b_6 ions. Labels are the same as in Figure 1.

Figure 2b) is that when photodissociation occurs inside the ion trap b_6, b_6* (NH_3 loss of b_6), and a_7 ions are also formed. Formation of these additional ions can be attributed to the extra time available for photofragment ions to undergo secondary fragmentation processes [32]. To confirm our assignments, b_6 + 2 ions were isolated inside the trap and collisionally dissociated. Major peaks in the MS^3 spectrum (Figure 2c) can all be interpreted as fragment ions arising from b_6 + 2 ions. In particular, product ions retaining the C-terminal histidine residue appear 2 Da higher than their conventional masses (b_6* − H_2O + 2, RVYIH + 2, and RVYIH − H_2O + 2), whereas three other assignable peaks that do not contain the histidine residue (b_4, b_4*, and VYI) are not shifted. This indicates that the 2 Da mass increase in b_6 + 2 ions is associated with histidine, which is the residue next to proline. For comparison, b_6 ions were also isolated and collisionally dissociated. As seen in Figure 2d, all peaks in the MS^3 spectrum can be assigned as product ions formed from b_6 ions, and no product ions show a 2 Da mass shift.

The effect of varying the ion extraction time in the TOF instrument following photofragmentation was also investigated. Figure S1 in Supplementary Information, which can be found in the electronic version of this article, displays 157 nm photodissociation mass spectra of singly-protonated angiotensin II (DRVYIH**P**F) recorded on LIT/o-TOF mass spectrometer with four different time delays between photoexcitation and ion extraction in the TOF source. At 300 ns (Figure S1a), the b_6 + 2 ion is comparable to the a_7 + 1 ion, and slightly less intense than the a_6, a_6 + 1, and a_6 + 2 ions. The tandem mass spectrum recorded with a 1 μs ion extraction delay is quite similar (Figure S1b). A minor difference between the two is an increase of the peak intensity of the a_6 ion. This may be attributed to loss of a hydrogen atom from the a_6 + 1 ion and/or secondary thermal fragmentation processes of large prompt photofragment ions. At a 5 μs delay (Figure S1c), the relative peak intensities among different ions are still similar, though the intensity of the a_6 ion increases slightly. Finally, at 13 μs (Figure S1d) b_6 and a_7 ions become apparent. This is somewhat similar to the Figure 2b spectrum. In conclusion, the a_n + 2 and b_n + 2 ions associated with proline are formed within 300 ns after photoexcitation and their abundances show little change up to 13 μs after laser irradiation.

Finally, to test the influence of precursor ion internal energy [43, 44] on the formation of b + 2 ions, DRVYIH**P**F and RDL**P**FF**P**V**P**ID were also photodissociated in a MALDI TOF-TOF mass spectrometer, and the resulting spectra appear in Figure 3. Instead of the b + 2 ions of Figure 1c and d, only conventional b-type ions appear in both spectra (b_6 in Figure 3a, and b_3, b_6, and b_8 in Figure 3b). It is well known that a vacuum MALDI ion source generates internally hot precursor ions [45, 46]. This suggests that b + 2 ions arise from precursor ions with low internal energies. In summary, b + 2 ions are not artifacts but stable fragment ions and their formation requires both precursor ions having low internal energies and a rapid non-thermal activation process.

Gas-Phase Structure of Proline

The unusual product ions associated with proline residues can be explained by considering the gas-phase structure of proline-containing peptides. The bulky and

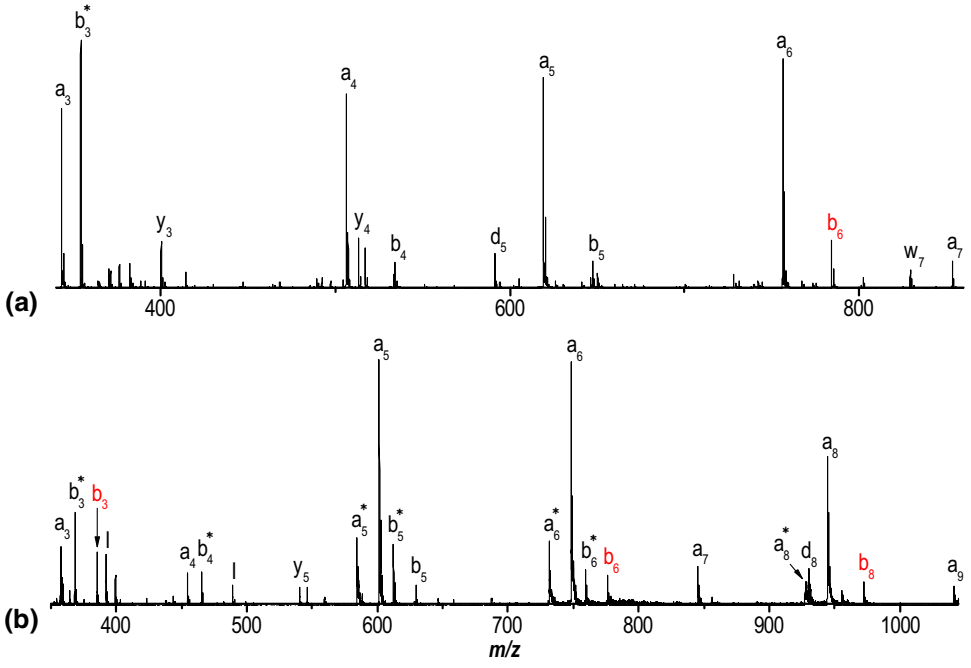

Figure 3. 157 nm photodissociation tandem mass spectra of (**a**) DRVYIH**P**F (angiotensin II), (**b**) RDL**P**FF**P**V**P**ID recorded with a MALDI TOF-TOF mass spectrometer.

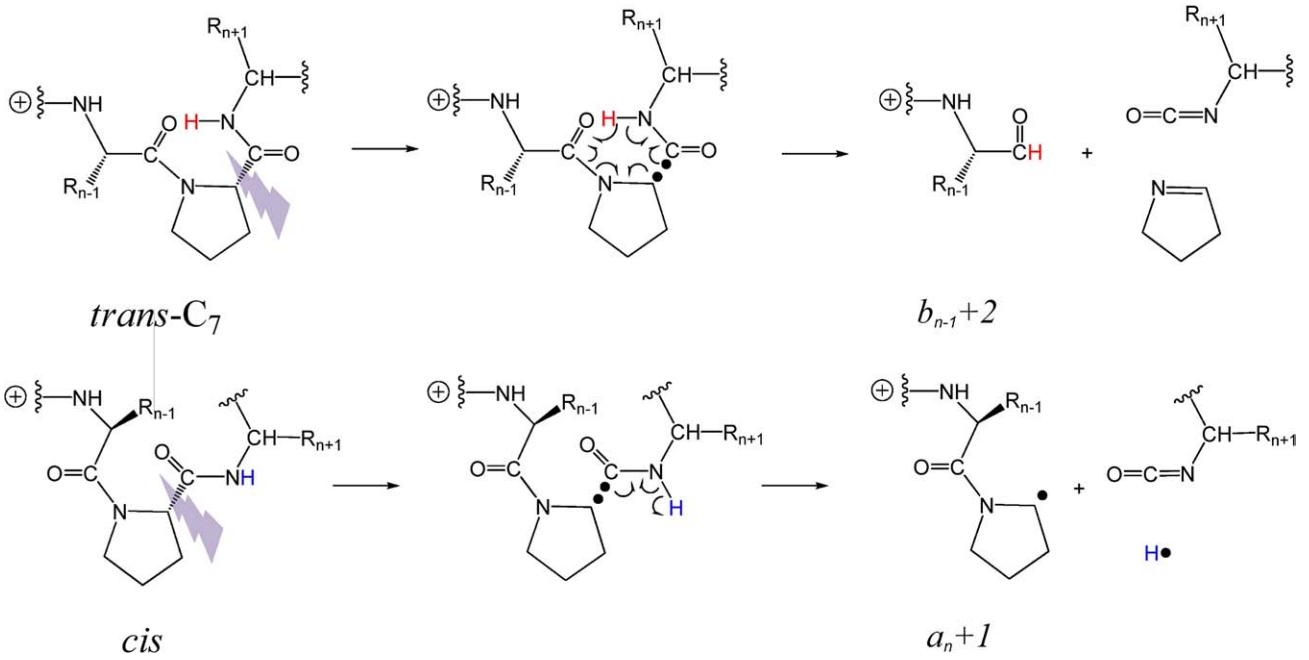

Scheme 1. A proposed mechanism for the formation of b_{n-1} + 2 and a_n + 1 ions for proline-containing peptides by 157 nm photodissociation.

rigid pyrrolidine ring of proline is unique among the amino acids and it imposes significant steric hindrance on the orientation of the preceding amino acid residue. It also fixes the dihedral angle ϕ at about $-60°$ [47]. Therefore, the rotational angle about the $C_\alpha-C$ bond (ψ) is the major factor that determines the conformational energy of an isolated proline residue with a *cis* or *trans* imide bond. N-acetyl-L-prolinamide ($AcProNH_2$) has been widely employed as a prototype model for a proline residue in peptides or proteins [48–50]. The most stable gas-phase conformation of $AcProNH_2$ has been found to be the internally hydrogen-bonded *trans*-C_7 structure ($\phi \approx -80°$, $\psi \approx 80°$), but a stable *cis* conformer ($\phi \approx -90°$, $\psi \approx -10°$) also exists [51, 52]. Assuming that these are the two main gas-phase structures of proline before photodissociation, plausible

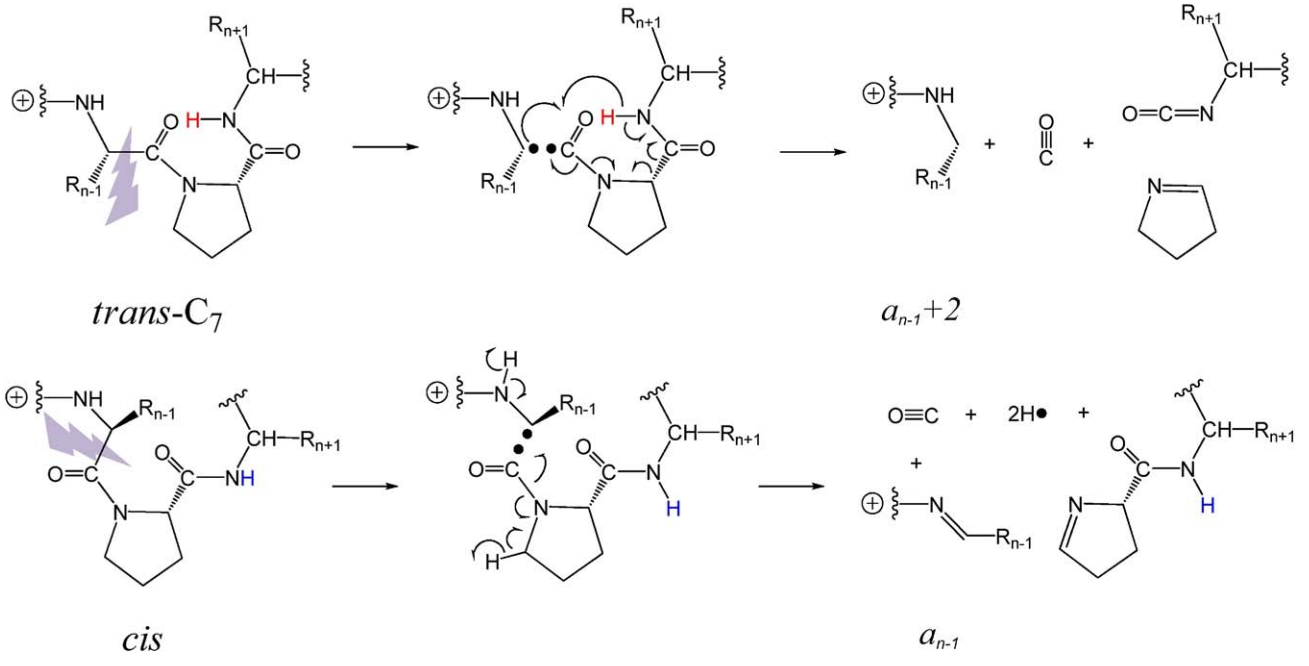

Scheme 2. A proposed mechanism for the formation of a_{n-1} + 2 and a_{n-1} ions for proline-containing peptides by 157 nm photodissociation.

mechanisms for the formation of $b + 2$ and $a + 2$ ions associated with proline in peptides are shown in Scheme 1 and Scheme 2, respectively. Although it is difficult to represent a three-dimensional structure in a two-dimensional picture, clearly the *trans*-C_7 form has an internal hydrogen bond while the *cis* form does not.

When proline is the nth residue from the N-terminus of a peptide, the carbonyl oxygen of the (n − 1)th residue makes a hydrogen bond to the amide hydrogen of the $(n + 1)^{th}$ residue in the *trans*-C_7 structure (Scheme 1). After light activation cleaves the bond between the α- and carbonyl-carbons of the nth proline residue, the two radical species formed can undergo electron rearrangement. Transfer of the amide hydrogen leads to formation of the observed $b_{n-1} + 2$ ions. In the *cis*-conformation, the hydrogen transfer is not possible because of the location of the amide hydrogen of the $(n + 1)^{th}$ residue. As shown in Scheme 1, $a_n + 1$ ions are then generated. The *trans*-conformation can also lead to the formation of $a + 2$ ions if the C_α−C bond N-terminal to proline is photodissociated as depicted in Scheme 2. Cleavage of this bond generates two radical species N-terminal to the proline residue. In the *trans*-C_7 structure, hydrogen transfer from the amide of the $(n + 1)^{th}$ residue to the α-carbon of the (n − 1)th residue results in $a_{n-1} + 2$ ions. Since this hydrogen transfer is not possible in the *cis*-conformation, photodissociation at the (n − 1)th residue produces normal a_{n-1} ions as shown in Scheme 2. Product ions associated with gas-phase proline structures generated by VUV photodissociation are summarized in Table 1.

Schemes S1 and S2 in Supplementary Information display the fragmentation that would be expected if the charge were located at the C- rather than the N-terminus. The mechanisms shown in Schemes S1 and S2 are similar to those in Schemes 1 and 2 above, but because the charge is on the C-terminal fragment, the ions observed are different. When proline is the mth residue from the C-terminus, photodissociation of the bond between the α- and carbonyl-carbons of the proline residue (Scheme S1) should yield x_{m-1} ions for both *trans*-C_7 and *cis* structures (although for the *cis* structure, $x_{m-1} + 1$ ions could be generated if the hydrogen is retained on the amide nitrogen after photodissociation). Photodissociation of the C_α−C bond in the residue N-terminal to proline (Scheme S2) leads to x_{m-1} and Y_m (2Da lighter than y_m) ions for the *trans*-C_7 and *cis* structures, respectively. All of these ion fragments have been observed in previous photofragmentation studies, so studies of peptide ions with C-terminal arginine were not conducted in the LIT/o-TOF photofragmentation apparatus.

Table 1. Product ions specific to the conformations of proline in the gas phase by 157 nm photodissociation in an ESI LIT/o-TOF mass spectrometer

Photodissociation site[a]	(n − 1)th residue[b]		nth residue[b]	
Proline Conformation	*trans*-C_7	*cis*	*trans*-C_7	*cis*
Type of Product Ions	$a_{n-1} + 2$	a_{n-1}	$b_{n-1} + 2$	$a_n + 1$

[a]Bond cleavage between the α- and carbonyl-carbons.
[b]Proline is assumed to be the nth residue from the N-terminus.

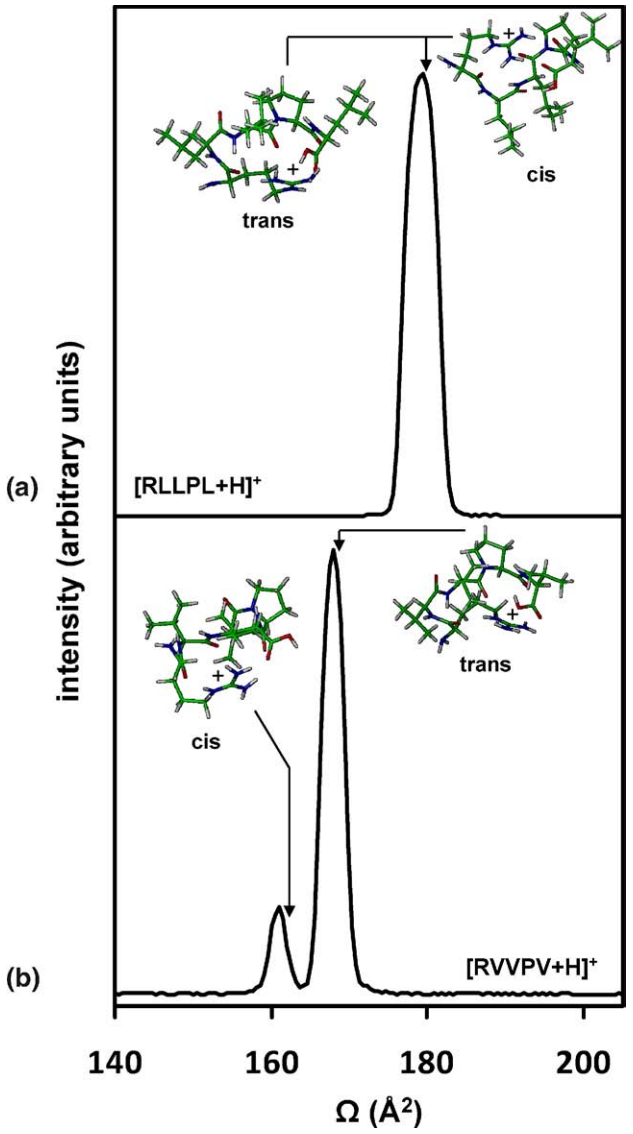

Figure 4. Drift time distributions plotted on a collision cross section scale for the peptide ions (**a**) [RLL**P**L + H]$^+$ and (**b**) [RVV**P**V + H]$^+$. Low-energy structures obtained from molecular dynamics simulations are provided as figure insets. Calculated collision cross sections for trial structures are indicated with arrows.

Photodissociation of singly-charged LLVVY**P**WTR by VUV light in the LIT/o-TOF mass spectrometer generates x_3, $x_3 + 1$, and Y_4 ions associated with the proline residue as shown in Supplementary Figure S2. As in our previous observations, x_4 ions are not observed in the spectrum. These results are consistent with the photodissociation mechanisms proposed in Schemes S1 and S2. Formation of y_4 ions can be ascribed to secondary thermal fragmentation processes of large prompt photofragment ions.

Comparison of VUV Photodissociation with IMS

Observation of two different gas-phase structures of proline-containing peptides is consistent with previous ion mobility results [26], in which multiple features are resolved. To investigate the differences between IMS and 157 nm photodissociation in probing the gas-phase conformations of proline, two small proline-containing peptides (RLL**P**L and RVV**P**V) were analyzed by both techniques. Figure 4a shows the drift time distribution for the peptide ion $[RLL\mathbf{P}L + H]^+$ plotted on a collision cross section scale. Here a single, broad feature is observed with a collision cross section centered at 179.4 Å^2. Shown in Figure 4b is the distribution obtained for the $[RVV\mathbf{P}V + H]^+$ ion in which two features are present. The high- and low-mobility ions are determined to have collision cross sections of 161.1 and 167.9 Å^2. In all simulated annealing runs, the lowest energy structures generated matched experimental collision cross sections to within 1.0%. Figure 4 presents a comparison of the calculated collision cross sections for low-energy structures (*cis*- and *trans*-configurations) and the experimental mobility distributions. In these studies the *cis*- and *trans*-configurations are more distinguished for the $[RVV\mathbf{P}V + H]^+$ ion than for the $[RLL\mathbf{P}L + H]^+$ ion. For example, on average, the percent difference between cross sections generated for the two different configurations is ~4.1% for the former peptide ion with the smaller value always comprised of the *cis*-configuration. This is nearly identical to the difference in sizes (4.22%) of the two dataset features observed in Figure 4b for this peptide ion. In comparison, the average percent difference for the two configurations of the $[RLL\mathbf{P}L + H]^+$ ion is ~0.5%.

Ion activation studies were used to determine the gas-phase equilibrium distribution of the two conformations observed for the $[RVV\mathbf{P}V + H]^+$ ion. Figure 5 shows the fraction of each conformation remaining as a function of voltage applied to the ion activation region.

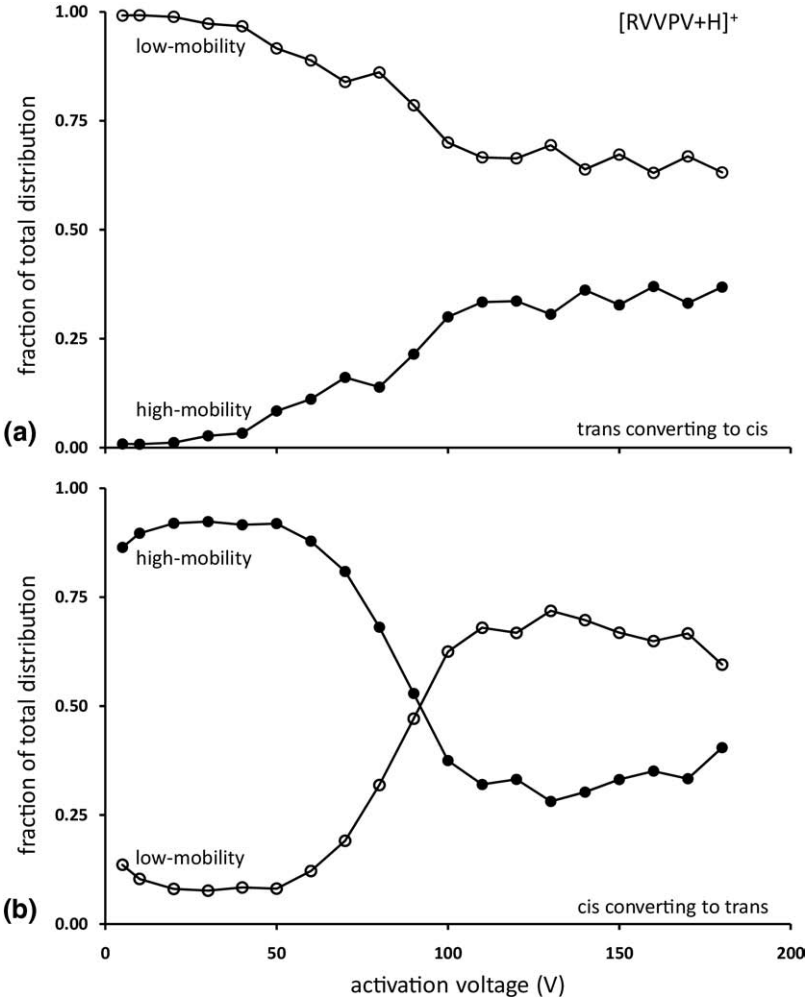

Figure 5. Plots of the fractions of the high- and low-mobility conformations observed in datasets as a function of ion activation voltage. Plots (**a**) and (**b**) represent datasets for which the low- and high-mobility species, respectively, are selected for ion activation. Based on molecular dynamics simulations, it is proposed that these respective plots represent (**a**) the *trans*-to-*cis* and (**b**) the *cis*-to-*trans* conversions of the proline residue configuration.

The measurements have been performed both for the selection of the low-mobility (Figure 5a) and the high-mobility (Figure 5b) conformations. The initial selection (low activation voltages) of the high mobility conformation reveals a small amount of the low-mobility ion (Figure 5b). Because these ions are nearly baseline resolved and the mobility selections have been performed in a fashion to minimize overlap (selecting edges of the peaks), it is proposed that the resulting low-mobility ions result from interconversion of the high- and low-mobility conformations in remaining regions of the drift tube. The application of increasing voltage to the ion activation region does not alter the fractions of the two conformations until a threshold value of 50 V is attained. From here an increase in the low-mobility conformation is observed with a corresponding decrease in the high-mobility conformation. This trend continues until the low-mobility conformation becomes the dominant dataset feature. Above 100 V, the fractions of each conformation remain relatively constant at ~0.67 and 0.33 for the low- and high-mobility conformations, respectively. For the low-mobility conformation (Figure 5a), a monotonic decrease in the selected ion is observed at low voltage. As before, the fractions of the two conformations level off at approximately a 2:1 ratio (low to high-mobility) above 100 V. In conclusion, ion mobility experiments demonstrate that the less compact, low mobility *trans*-conformation of $[RVV\mathbf{P}V + H]^+$ is more stable than its more compact, high mobility *cis*-conformation.

Figure 6 displays VUV photodissociation of $[RVV\mathbf{P}V + H]^+$ and $[RLL\mathbf{P}L + H]^+$ ions recorded on the hybrid mass spectrometer with a time delay of 5 μs between laser irradiation and ion extraction in the TOF source.

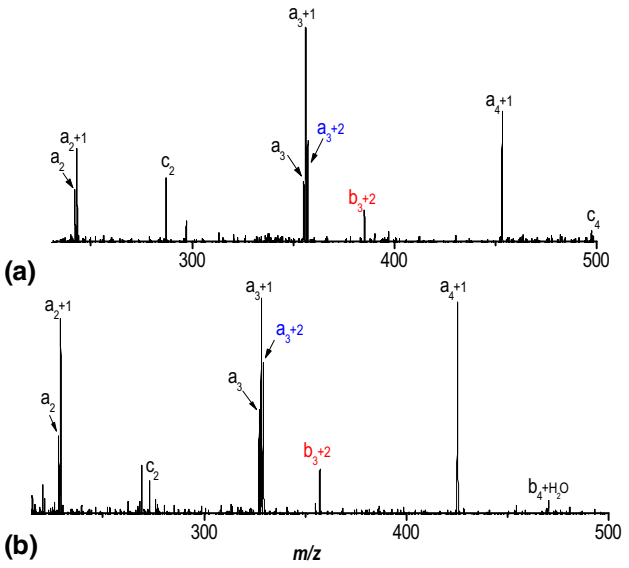

Figure 6. 157 nm photodissociation of mass spectra of singly-protonated (**a**) RLL**P**L and (**b**) RVV**P**V recorded with LIT/o-TOF mass spectrometer with a time delay of 5 μs between laser irradiation and ion extraction in the TOF source.

Both peptides generate a pair of $b_3 + 2$ and $a_3 + 2$ ions associated with the *trans*-C_7 conformation of the proline residue. In contrast with ion mobility experiments, the photodissociation experiment distinguishes the two conformations of proline based on different product ions in a mass spectrum rather than as two peaks in a drift time dimension. In the ion mobility studies, not all proline-containing peptides exhibit multiple features due to the limited resolution of the method as demonstrated in Figure 4. In contrast, the two conformations of proline are always evident in photodissociation mass spectra recorded with the hybrid instrument. In addition, for peptides containing multiple proline residues, photodissociation generates product ions specific to the conformation of each proline residue in a peptide as shown in Figure 1d. It is noteworthy that the peak intensity ratio of $b_3 + 2$ (*trans*-C_7) to $a_4 + 1$ (*cis*) in Figure 6b is about 1:4, while the ratio of the *trans*- to the *cis*-conformations is ~2:1 in the IMS experiments (Figure 5). The latter ratio probably reflects the relative stability of the *trans*- and *cis*-conformations while the former apparently does not. This discrepancy can be explained by considering the conditions under which $b_3 + 2$ ions are formed. Generation of $b_3 + 2$ ions require a hydrogen transfer following photodissociation. This hydrogen transfer is possible through the intramolecular hydrogen bond formed only when the imide bond of proline is *trans* ($\omega \approx 180°$) *and* $\psi \approx 80°$. Thus, some of *trans*-conformations of proline that have ψ values significantly different from 80° will result in $a_4 + 1$ ions, instead of $b_3 + 2$ ions. In addition, the formation of $b_3 + 2$ ions would be even lower if the hydrogen transfer efficiency between the amino acid residues adjacent to proline is not as efficient as 100%. In summary, a peak ratio of $b_3 + 2$ to $a_4 + 1$ ions in Figure 6 can be interpreted as a fraction of the *trans*-C_7 to all other conformations of the proline.

Implications of the trans-C_7 *conformation in 'Proline Effect'*

As noted above, Wysocki and coworkers have found that the residue N-terminal to proline in a peptide ion affects the propensity for cleavage between the two [31]. They suggested that some *trans*-conformation may be involved in facilitating this process. Schemes **1** and **2** clearly display how the *trans*-C_7 conformation could play this kind of role [53, 54]. However, a mobile proton is almost certainly involved in the proline-induced cleavage of peptide ions and such a proton is not presently incorporated in this picture. Furthermore, the hydrogen bonding in the *trans*-C_7 conformation of proline is not expected to survive during low-energy collisional activation. Studying the effects of collisional activation and protonation on the stability of the hydrogen bonding in the *trans*-C_7 conformation of proline will be valuable to learn whether this *trans*-conformer can

38. Shvartsburg, A. A.; Jarrold, M. F. An Exact Hard-Spheres Scattering Model for the Mobilities of Polyatomic Ions. *Chem. Phys. Lett.* **1996,** *261,* 86–91.
39. Thompson, M. S.; Cui, W.; Reilly, J. P. Fragmentation of Singly Charged Peptide Ions by Photodissociation at $\lambda = 157$ nm. *Angew. Chem. Int. Ed.* **2004,** *43,* 4791–4794.
40. Cui, W.; Thompson, M. S.; Reilly, J. P. Pathways of Peptide Ion Fragmentation Induced by Vacuum Ultraviolet Light. *J. Am. Soc. Mass Spectrom.* **2005,** *16,* 1384–1398.
41. Zhang, L. Y.; Cui, W.; Thompson, M. S.; Reilly, J. P. Structures of α-Type Ions Formed in the 157 nm Photodissociation of Singly-Charged Peptide Ions. *J. Am. Soc. Mass Spectrom.* **2006,** *17,* 1315–1321.
42. Zubarev, R. A.; Horn, D. M.; Fridriksson, E. K.; Kelleher, N. L.; Kruger, N. A.; Lewis, M. A.; Carpenter, B. K.; McLafferty, F. W. Electron Capture Dissociation for Structural Characterization of Multiply Charged Protein Cations. *Anal. Chem.* **2000,** *72,* 563–573.
43. Gabelica, V.; Schulz, E.; Karas, M. Internal Energy Build-Up in Matrix-Assisted Laser Desorption/Ionization *J. Mass Spectrom.* **2004,** *39,* 579–593.
44. Gabelica, V.; De Pauw, E. Internal Energy and Fragmentation of Ions Produced in Electrospray Sources. *Mass Spectrom. Rev.* **2005,** *24,* 566–587.
45. Spengler, B.; Kirsch, D.; Kaufmann, R. Metastable Decay of Peptides and Proteins in Matrix-Assisted Laser-Desorption Mass-Spectrometry. *Rapid Commun. Mass Spectrom.* **1991,** *5,* 198–202.
46. Spengler, B. Post-Source Decay Analysis in Matrix-Assisted Laser Desorption/Ionization Mass Spectrometry of Biomolecules. *J. Mass Spectrom.* **1997,** *32,* 1019–1036.
47. Schimmel, P. R.; Flory, P. J. Conformational Energies and Configurational Statistics of Co-Polypeptides Containing L-Proline. *J. Mol. Biol.* **1968,** *34,* 105–120.
48. Ramek, M.; Kelterer, A. M.; Teppen, B. J.; Schafer, L. Theoretical Structure Investigations of N-Acetyl-L-Proline Amide. *J. Mol. Struct.* **1995,** *352,* 59–70.
49. Zanni, M. T.; Gnanakaran, S.; Stenger, J.; Hochstrasser, R. M. Heterodyned Two-Dimensional Infrared Spectroscopy of Solvent-Dependent Conformations of Acetylproline-NH_2. *J. Phys. Chem. B* **2001,** *105,* 6520–6535.
50. Hahn, S.; Lee, H.; Cho, M. Theoretical Calculations of Infrared Absorption, Vibrational Circular Dichroism, and Two-Dimensional Vibrational Spectra of Acetylproline in Liquids Water and Chloroform. *J. Chem. Phys.* **2004,** *121,* 1849–1865.
51. Lee, K. K.; Hahn, S.; Oh, K. I.; Choi, J. S.; Joo, C.; Lee, H.; Han, H. Y.; Cho, M. Structure of N-Acetylproline Amide in Liquid Water: Experimentally Measured and Numerically Simulated Infrared and Vibrational Circular Dichroism Spectra. *J. Phys. Chem. B* **2006,** *110,* 18834–18843.
52. Sul, S.; Karaiskaj, D.; Jiang, Y.; Ge, N. H. Conformations of N-Acetyl-L-Prolinamide by Two-Dimensional Infrared Spectroscopy. *J. Phys. Chem. B* **2006,** *110,* 19891–19905.
53. O'Hair, R. A. J. The Role of Nucleophile-Electrophile Interactions in the Unimolecular and Bimolecular Gas-Phase Ion Chemistry of Peptides and Related Systems. *J. Mass Spectrom.* **2000,** *35,* 1377–1381.
54. Wysocki, V. H.; Tsaprailis, G.; Smith, L. L.; Breci, L. A. Special Feature: Commentary—Mobile and Localized Protons: A Framework for Understanding Peptide Dissociation. *J. Mass Spectrom.* **2000,** *35,* 1399–1406.